International Journal of Pressure Vessels and Piping 212 (2024) 105358

Contents lists available at ScienceDirect

International Journal of Pressure Vessels and Piping

journal homepage: www.elsevier.com/locate/ijpvp

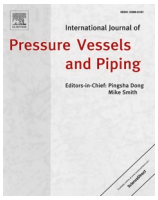

A comprehensive finite element framework for modeling of PEX-Al-PEX composite pipes

Ameer Alaa Oleiwi, Hamed Afrasiab *, Abbas Zolfaghari

Mechanical Engineering Department, Babol Noshirvani University of Technology, Babol, Iran

ARTICLE INFO

Keywords:
PEX-Al-PEX composite pipes
Finite element method
Mechanical behavior
Temperature
Strain-rate

ABSTRACT

While PEX-Al-PEX composite pipes are widely used in various applications, suitable tools and models for simulating their performance under different working conditions have not been made available. Therefore, the present study aims to develop a comprehensive finite element model to study the behavior of PEX-AL-PEX pipes at different temperatures and strain-rates. To achieve this, the properties of the pipe layers have been obtained for different temperature and strain-rate values through experimental tests. To assess the accuracy of the developed finite element model, the lateral compression and the split-disc tension tests have been performed under different conditions using both experimental and finite element analysis methods, and their results have been compared. The proposed model can be used to study the behavior of PEX-AL-PEX pipes with different materials and geometries in various conditions and applications, as well as for optimizing the design and manufacturing of these pipes.

1. Introduction

Over the past few decades, composite pipes have been increasingly used in various industries and applications due to their exceptional properties [1–3]. These pipes combine lightweight with high strength and stiffness, and exhibit good thermal properties, excellent resistance to corrosion, extended service life, decreased maintenance and use costs, and a host of distinctive attributes in comparison to traditional plastic and metal pipes [4–6].

Among the composite pipes, the ones with multilayered structure are manufactured using a well-engineered combination of several layers. Each layer is made of a selected material to provide a specific feature. With this composite of high-quality materials, multilayer pipes can be strong and stable similar to metal pipes, while maintaining lightweight, ease of shaping, cutting and installation akin to plastic pipes [7–9].

Multilayered composite pipes find their primary application in water and gas transportation, but they also serve a wide range of other purposes. These include use in fuel oil lines, compressed air systems, solar heating, food/chemical processing, air conditioning, refrigerant systems, air conditioning, underfloor heating and more [10–12]. This wide application has encouraged several studies to investigate different properties of these pipes. Hutar et al. [13] used fracture mechanics to analyze the effect of a cracked protective layer on the integrity of multilayer composite pipes. Niedermayer and Frankenheim [14] employed the field matching technique to analytically calculate longitudinal and transverse resistive wall impedances of a circular multilayer pipe. Aguiar et al. [15] proposed a new finite element model to study the behavior of three-dimensional multilayered pipe in pipeline applications. Sarvestani and Hojjati [16] presented a new method based on Toroidal Elasticity to study curved pipes made of thick laminated composite subjected to mechanical loadings. Bai et al. [17] employed the finite element model of a multilayered flexible pipe to analyze the mechanical response of the internal cylinder when subjected to external pressure and being confined by outer cylinders. Hartmann et al. [18] proposed an analytical solution for multilayered thick-walled tubes under constant axial deformation, internal and external pressure using small strain thermo-elasticity theory. Wu et al. [19] used elasticity equations to find analytical solutions for the stresses and displacements in each layer of an infinite multilayer pipe bonded by viscoelastic interlayer. Zhang et al. [20] used thermo-elasticity theory to determine displacement, stress, and temperature fields in a multilayered pipe with temperature-dependent properties subjected to thermal load and non-uniform pressure. Dong et al. [7] employed large deformation finite element simulations to explore the effect of multilayer pipeline-backfill-trench interaction on the soil pressure on the pipe and deformation of the pipe section. Travnicek et al. [21] developed

* Corresponding author.
E-mail address: afrasiab@nit.ac.ir (H. Afrasiab).

https://doi.org/10.1016/j.ijpvp.2024.105358
Received 16 September 2024; Received in revised form 13 October 2024; Accepted 5 November 2024
Available online 7 November 2024

numerical simulations coupled with lifetime estimations to study the performance of a multilayered pipe formed by sandwiching a recycled high-density polyethylene (HDPE) layer between two protective layers made of virgin HDPE.

One of the most popular types of multilayer pipes is the PEX-Al-PEX (cross-linked polyethylene-aluminum-cross-linked polyethylene) composite pipe which finds extensive use in plumbing, heating, and cooling systems within buildings. This type of pipe consists of three primary layers: an inner and outer layer of PEX, with a layer of aluminum sandwiched between them. A polyethylene adhesive is applied between the layers to securely bond the aluminum layer to the inner and outer PEX layers. The inclusion of the aluminum layer significantly enhances the pipe's strength, stiffness, stability, and durability. It also results in a higher temperature and pressure rating, as well as reduced expansion and contraction. Additionally, the aluminum layer serves as an effective oxygen barrier, reducing the risk of corrosion, scaling, and deterioration of water quality.

Despite the widespread use of PEX-Al-PEX pipes, there is a limited amount of research available in the open literature regarding their mechanical properties and behavior. Specifically, the authors identified only two relevant articles in the existing body of research. Riahi and Ebrahimi [22] proposed an apparatus for the online evaluation of the aluminum layer seam weld in PEX-AL-PEX pipes by using an inductive proximity sensor. Atarodi Kashani et al. [23] conducted experiments to assess the long-term performance of PEX multi-layer pipes over a duration of 1000 h, considering various pipe diameters and two different welding types, namely, tungsten inert gas and ultrasonic welding. They also employed classical elasticity theory to carry out an analysis for hoop and radial stresses within the layers of the pipe. In both of mentioned studies, the main focus was placed on the seam weld of the aluminum layer, and the material properties of the pipe layers were not considered in detail. Furthermore, an elaborated modeling strategy was not presented in these studies.

To address this gap in the literature, a comprehensive finite element framework is developed here in the Abaqus/explicit software for modeling the mechanical behavior of PEX-Al-PEX composite pipes in various working conditions. To achieve this, the properties of the pipe PEX and aluminum layers have been obtained for different values of temperature and strain-rate through experimental tests and other valid methods. Subsequently, these properties have been implemented using available models in the Abaqus default library and by writing a VUMAT subroutine. To assess the accuracy of the developed finite element model, two standard tests, the lateral compression test and the split-disc tension test, have been performed under different conditions using both experimental and finite element analysis methods, and their results have been compared. Furthermore, the radial and circumferential stress distributions in the pipe under two different pressures have been obtained using the finite element model and compared with the results of an analytical method presented in Ref. [23]. Details of the experimental and finite element methods are shown in the subsequent sections.

2. Materials and methods

In this section, first the geometric dimensions of the pipe are accurately measured and detailed in part 2.1. The dimensions of the pipe are manufactured according to the standard. However, the diameter and thickness of the pipe layers have specified tolerances as per the relevant standard and these dimensions may vary slightly in different segments of the pipe. Therefore, precise measurement of these dimensions is essential for accurate modeling.

In Parts 2.2 to 2.4, constitutive equations for modeling the deformation behavior of the pipe components are proposed and compared with experimental stress-strain curves at different temperatures and strain-rates. The experimental properties of the PEX and adhesive layers under the desired operating conditions were obtained from their manufacturers and are presented in Parts 2.3 and 2.4. However, the experimental stress-strain curves for the aluminum layer at various temperatures and strain-rates were not provided by its manufacturer. Although the employed aluminum is standardized, there may be some degree of variation between the properties of sheets produced by different manufacturers. Therefore, a sample of the sheet used in the pipe was obtained from the pipe manufacturer, and its stress-strain curve under different operating conditions was extracted as explained in Part 2.2.

2.1. Pipe dimensions

To carry out the studies, two PEX-Al-PEX pipe branches with standard sizes of 2025 and 2532 (according to ASTM f1281 [24]) were obtained from the associated manufacturing company. To determine the precise dimensions of the pipes, the inner and outer diameters were measured using a caliper on various cut pieces of each branch after cutting them to appropriate lengths. Observations showed that the inner and outer diameters vary slightly along the length of each branch. Therefore, in accordance with Table (1), average values were used to report these dimensions.

To determine the layers thickness accurately, various cuts of the pipe were imaged under a 20× optical microscope. Examples of these images are shown in figure (1). The thickness values differed slightly across different sections, and the average values are reported in Table (2).

To create geometry of models in finite element simulations, average sizes given in tables (1) and (2) were used.

2.2. Properties and constitutive modeling of the aluminum layer

A commonly used material for the production of PEX-Al-PEX pipes is the aluminum alloy 3003. To obtain the properties of this alloy, a piece of aluminum 3003 sheet was obtained from the pipe manufacturer and test specimens were made using the wire-cutting method for tension testing according to the ASTM E8/E8M standard [25]. The standard dimensions of the samples and an image of a fabricated sample are shown in figures (2) and (3).

The tension test was performed for aluminum samples in different strain-rates of 0.001/s, 0.01/s, 0.1/s, and 1.0/s at T = 20°C and different temperatures of 20, 50, 75, and 100°C at strain-rate of 0.001/s. Each test was replicated three times according to ASTM E8/E8M standard. An image of two fractured specimens after the tensile test is shown in figure (4).

For defining the plastic behavior of aluminum and its alloys which is dependent on the plastic strain, strain-rate and temperature, adopting the Johnson-Cook constitutive model is very popular [26–30]. In the Johnson–Cook equation, the flow stress of the material is expressed as [31–34]:

$$\sigma_Y = \left(A + B\varepsilon_p^n\right)\left(1 + C\ln\bar{\varepsilon}_{,t}\right)\left(1 - \overline{T}^m\right) \quad (1)$$

where σ_Y, ε_p, and T_{melt} are flow stress, plastic strain, and melting temperature of the material, respectively. A (in MPa) is the yield stress of the material at reference strain-rate and temperature, B (in MPa) and n represent the hardening modulus and work-hardening exponent, which describe the influence of strain hardening. C and m are the strain-rate hardening and thermal softening coefficient, respectively. The subscript "$,t$" under a variable indicates the time derivative of that

Table 1
The measured dimensions of the 2025 and 2532 pipes (in mm).

Nominal pipe size	Outside diameter range	Inside diameter range	Average Outside diameter	Average inside diameter
2025	25.1–25.9	19.8–20.4	25.5	20.1
2532	31.7–32.7	25.1–25.5	32.2	25.3

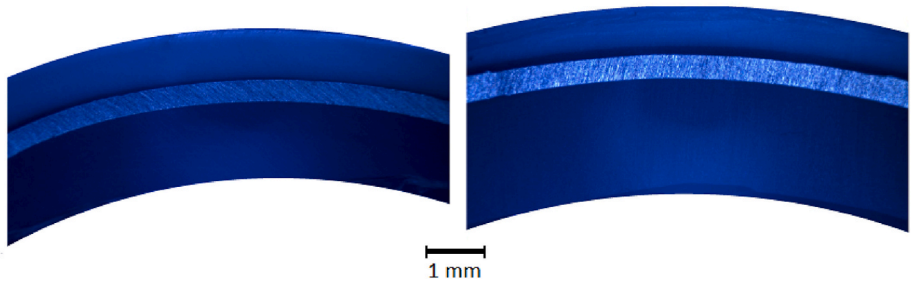

Fig. 1. A portion of PEX-Al-PEX pipes under optical microscope.

Table 2
The average measured thickness of layers (in mm).

Nominal pipe size	Outer PEX thickness	Aluminum thickness	Inner PEX thickness	Total thickness
2025	0.90	0.40	1.40	2.70
2532	0.90	0.45	2.10	3.45

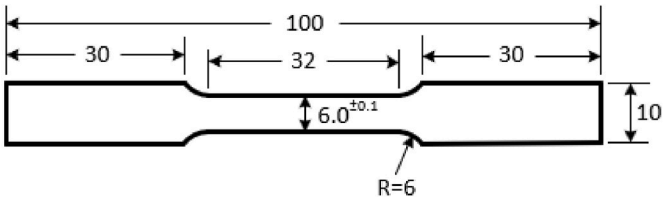

Fig. 2. Dimensions (in mm) of test samples according to ASTM E8/E8M standard.

Fig. 3. An aluminum sample made by wirecut for the tension test.

Fig. 4. Two aluminum 3003 samples after tensile test.

variable. The dimensionless strain-rate ($\overline{\varepsilon}_{,t}$) and temperature ($\overline{T}$) are defined as:

$$\overline{\varepsilon}_{,t} = \frac{\varepsilon_{,t}}{\varepsilon_{,t-\mathrm{ref}}}, \overline{T} = \frac{T - T_{\mathrm{ref}}}{T_{\mathrm{melt}} - T_{\mathrm{ref}}} \tag{2}$$

with respect to the reference strain-rate ($\varepsilon_{,t-\mathrm{ref}}$) and reference temperature (T_{ref}). The melting temperature for aluminum 3003 alloy is $T_{\mathrm{mlet}} =$ 650°C as indicated in Refs. [35–37].

By adopting the linear elastic model before yielding and Johnson-Cook model after it, the following constitutive relationship has been used for the aluminum layer in this study:

$$\begin{cases} \sigma = E\varepsilon \quad \text{if} \quad \sigma \le \sigma_{Y0} \\ \sigma = \left(A + B\varepsilon_p^n\right)\left(1 + C\ln\overline{\varepsilon}_{,t}\right)\left(1 - \overline{T}^m\right) \quad \text{if} \quad \sigma > \sigma_{Y0} \end{cases} \tag{3}$$

The experimental stress-strain curves of aluminum samples were employed for determining the unknown parameters of the Johnson-Cook model. To this end, $T_{\mathrm{ref}} = 20^{\circ}\mathrm{C}$ and $\varepsilon_{,t-\mathrm{ref}} = 0.001$ mm/s have been selected as the reference temperature and strain-rate, respectively. By fitting different parts of equation (3) to experimental data, values listed in Table (3) were obtained for properties of the aluminum layer.

The value of $\nu = 0.33$ has been selected for Poisson's ratio, which is a typical value for aluminum and its alloys [38–41].

The ductile damage model has been used to predict the fracture of the aluminum layer in the finite element simulations. In this model, failure occurs when the plastic strain reaches a critical value called fracture strain. The value of the fracture strain is a function of the strain-rate and temperature and is obtained from the experimental stress-stress curve. At any time in the damage process, the stress tensor of the material (σ) is given by the scalar damage equation:

$$\sigma = (1 - D)\overline{\sigma} \tag{4}$$

Therein, D is the overall damage variable and $\overline{\sigma}$ is the effective stress tensor calculated in the current increment. In other words, $\overline{\sigma}$ is the stress that would exist in the material in the absence of damage. When $D = 1$, the material loses its bearing capacity. By default, if all cross-section points at any integration location lose their load-bearing capacity, an element is deleted from the grid.

To examine the validity of the developed material model, several tension tests have been implemented in the finite element software for different strain-rates and temperatures according to the ASTM E8/E8M. The predictions made by the developed model are compared with experimental data in figures (5) and (6), respectively.

As these figures suggest, the developed material model is capable of predicting the stress-strain behavior of the aluminum layer in different conditions by suitable accuracy.

2.3. Properties and constitutive modeling of PEX layers

The experimental stress-strain curves of the PEX material used in the manufacturing of the PEX-Al-PEX pipe were obtained at selected strain-rates (0.001/s, 0.01/s, 0.1/s, and 1.0/s at T = 20°C) and temperatures (20, 50, 75, and 100°C at strain-rate of 0.1/s) from a company that supplies this material to the pipe manufacturer.

To develop the associated constitutive relations, it was noted that in several previous studies the dependence of the elastic and plastic properties of polyethylene materials on the strain-rate was described by power-law relations [42–44] and on temperature by exponential functions [45–47]. Therefore, in this study the following relations have been used to obtain the elastic modulus (E), initial yield stress (σ_{Y0}) and the tangential modulus of the stress-strain curve in the plastic deformation region (E^t) in a specific strain-rate and temperature:

Table 3
Material parameters of equation (3) obtained for the aluminum layer.

E (GPa)	A (MPa)	B (MPa)	C	n	m
68.9	154.67	57.17	0.0146	1.0	0.9984

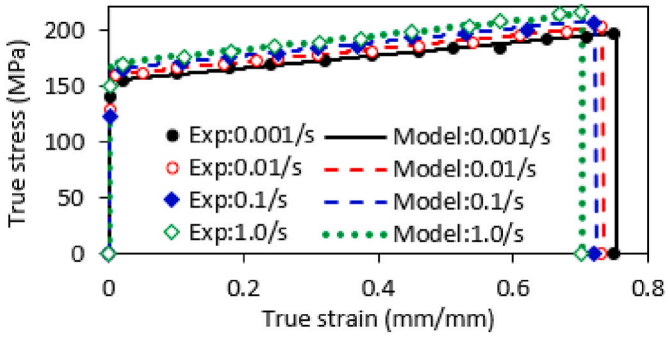

Fig. 5. Comparing the prediction of the aluminum 3003 material model with experimental data at different strain-rates.

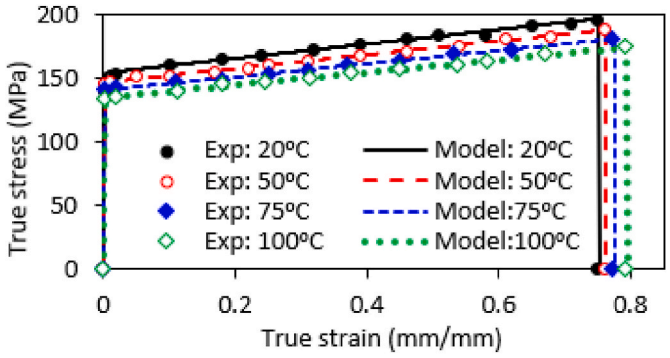

Fig. 6. Comparing the prediction of the aluminum 3003 material model with experimental data at different temperatures.

$$E = E_{\text{ref}}\left(1 + A_1\left(\bar{\varepsilon}_{,t}^{\,b_1} - 1\right)\right)e^{c_1\overline{T}} \tag{5}$$

$$\sigma_{Y0} = \sigma_{Y0-\text{ref}}\left(1 + A_2\left(\bar{\varepsilon}_{,t}^{\,b_2} - 1\right)\right)e^{c_2\overline{T}} \tag{6}$$

$$E^t = E^t_{\text{ref}}\left(1 + A_3\left(\bar{\varepsilon}_{,t}^{\,b_3} - 1\right)\right)e^{c_3\overline{T}} \tag{7}$$

where E_{ref}, $\sigma_{Y0-\text{ref}}$, and E^t_{ref} are the elastic modulus, initial yield stress and tangential modulus at the reference strain-rate and temperature, respectively. A, b, and c are material parameters that are obtained by fitting relations (5), (6), and (7) to experimental data.

By assuming an elastic-linearly hardening plastic model in which the stress and plastic strain are linearly dependent in the plastic deformation zone, the following constitutive relationship has been used to characterize the PEX material mechanical behavior:

$$\begin{cases} \sigma = E\varepsilon & \text{if} \quad \sigma \le \sigma_{Y0} \\ \sigma = \sigma_{Y0} + E_t\left(\varepsilon - \dfrac{\sigma_{Y0}}{E}\right) & \text{if} \quad \sigma > \sigma_{Y0} \end{cases} \tag{8}$$

Since the material behavior defined in equations (5)–(8) is not included as an option in the default material library of Abaqus, a VUMAT subroutine was developed to implement the material model given in these equations. The ductile damage model along with the element deletion option was also coded in the this VUMAT subroutine to simulate the fracture process of the PEX material. The fracture process was triggered in a certain fracture strain with damage variable start to increase from $D = 0$. The process continued and the damage variable increased linearly with the equivalent plastic strain to $D = 1$ where another fracture strain threshold is met and total fracture occurs. The values for fracture strains were obtained from experimental stress-strain curves of the PEX material at different strain-rates and temperatures.

In order to determine the associated material constants, these equations have been fitted to experimental data and the values obtained for these constants are listed in Tables (4) and (5).

To examine the validity of the proposed material model, tension tests according to the ASTM D638 [48] have been simulated in the finite element software at different strain-rates and temperatures. The results of the model are compared with experimental data in figures (7) and (8), respectively.

According to figures (7) and (8), the material model proposed for PEX can properly predict its properties in different conditions of strain-rate and temperature.

2.4. Properties and constitutive modeling of the adhesive material

For modeling the adhesive that binds different layers of the pipe together, the cohesive zone element and associated traction-separation law based on the maximum principal stress have been employed in Abaqus [49]. The adhesive used in the pipe was the ARIA adhesive 4107T242. The properties of this adhesive were taken from the supplier's catalogue and are presented in Table 6 at T = 20°C.

The thickness of the adhesive layer was assumed to be 0.01 mm [50–53]. Since the properties of adhesive were not specified at different temperatures and strain-rates, the effect of strain-rate on its properties was neglected. Furthermore, it was assumed that the mechanical strength and stiffness of adhesive decrease linearly from their initial values given in Table (6) at T = 20°C to about 10 % of their initial values at T = 102°C (Vicat softening point) based on information provided by the supplier. For this purpose, these properties were defined as temperature-dependent functions within the property module of Abaqus.

2.5. Modeling assumptions

Since different types of aluminum welding were comprehensively investigated in previous studies on PEX-Al-PEX pipes [22,23], for the sake of simplicity and to focus more on material properties, the presence of the weld seam in the aluminum layer of the pipe has been disregarded in finite element model. The experimental tests were also conducted such that the effect of the weld seam on the result was minimal.

Due to the significantly smaller deformation of the tools in comparison to the specimens, they were modelled as rigid bodies in all simulations. Owing to the symmetry present in the problems and for the purpose of reducing computational costs, one-eighth of the models were used in the simulations. Element types R3D4,[1] C3D8R,[2] and COH3D8[3] were used to mesh tools, PEX and aluminum layers, and cohesive layers, respectively.

The appropriate element size for performing the finite element simulations was determined by performing mesh independence study in each case. The results of the mesh independence study for the lateral compression test are presented in Table (7) for a test fixture speed of 0.1 mm/s and a temperature of 20 °C. In this table the maximum von Mises stress in the pipe at the maximum compressive displacement is listed against the element size of the pipe. Based on this table, the element size of 0.1 mm is appropriate for meshing the pipe model in the lateral compression test. The same mesh size was observed to be a suitable

Table 4
PEX properties at the reference strain-rate and temperature.

E_{ref} (MPa)	$\sigma_{Y0-\text{ref}}$ (MPa)	E^t_{ref} (MPa)
247	16.5	42

[1] A 4-node 3-D bilinear rigid quadrilateral.
[2] An 8-node linear brick, reduced integration, hourglass control.
[3] An 8-node three-dimensional cohesive element.

Table 5
Material parameters for the PEX material.

A_1	b_1	c_1	A_2	b_2	c_2	A_3	b_3	c_3
0.3	0.31	−2.6	185	1.8×10^{-4}	−1.4	−0.65	−0.3	−1.5

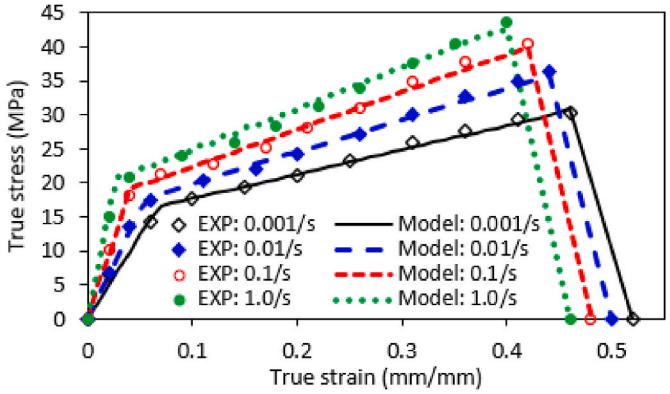

Fig. 7. Comparison of the PEX model prediction with experimental data at different strain-rates.

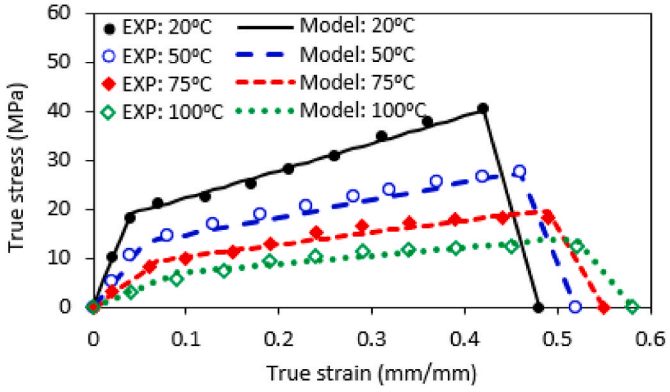

Fig. 8. Comparison of the PEX model prediction with experimental data at different temperatures.

Table 6
Average properties of the adhesive material.

Property	Value	Unit
Density	930	Kg/m3
Melting temperature	139	°C
Vicat softening point	102	°C
Elastic modulus	17	MPa
Tensile strain at break	400	%
Tensile stress at yield	14	MPa
Tensile stress at break	15	MPa

Table 7
Results of the mesh independence study for the lateral compression test.

Element size (mm)	Maximum von Mises stress in pipe (MPa)	Error (%)
2.0	127.2	22.1
1.0	163.2	18.0
0.5	199.0	−11.7
0.25	178.1	0.5
0.1	179.0	0.9
0.05	180.6	–

choice for other values of the fixture speed and temperature.

The results of a similar study for the split-disk test are presented in Table (8) for a test fixture speed of 0.1 mm/s and a temperature of 20 °C. According to this table, the element size of 0.1 mm is appropriate for modeling this test too. The mesh size of 0.1 mm was also found to be satisfactory for other values of the fixture speed and temperature.

A convergence study was also performed on the time step size of the simulations and it was observed that a step size of 5×10^{-5}s is suitable for all simulations.

It should also be noted that the operational range considered for the PEX-Al-PEX pipe in this study is a temperature range of 20-100°C and loading speed range of 0.001–1.0 mm/s. Therefore, caution should be exercised when applying the findings of this article to specific operating conditions outside of this defined range. For example, some mechanical properties of polymers degrade at temperatures above 150°C, leading to reduced stiffness and strength [54], which has not been considered in this study. Additionally, studying very high strain-rates, such as those resulting from a bullet impact on the pipe, may not be feasible with the models presented in this article.

3. Results and discussion

In this section, two standard tests, frequently used to evaluate pipe performance, are studied using both experimental and finite element methods, and their results are compared to validate the finite element model.

3.1. Pipe lateral compression test

One of the common tests for studying the mechanical behavior of pipes under different working conditions is the lateral compression test which has been widely used in many previous studies such as [55–57]. This test has been also used in the current research to analyze the behavior of PEX and PEX-Al-PEX pipes. For this purpose, compression samples were prepared with the length of 25 mm and internal diameter of 20 mm from 2025 PEX-Al-PEX pipe according to the geometry presented in Ref. [57]. To create single-layer samples of the PEX material, a PEX-Al-PEX pipe was machined [57] and its outer PEX and aluminum layers were removed, and the thickness of the inner PEX layer was reduced to 1 mm. The PEX and PEX-Al-PEX compression test samples are shown in figure (9). Snapshots of the PEX-Al-PEX pipe compression at different time points are also provided in figure (10). The tests have been performed at T = 20°C for four different speeds (0.001, 0.01, 0.1, and 1.0 mm/s) of the compressive test fixture, and at different temperatures (20, 50, 75, 100°C) for fixture speed of 0.1 mm/s. Each test was repeated on five specimens to obtain a reliable average for a sample.

The developed finite element model has been also used to simulate the lateral compression test of PEX and PEX-AL-PEX pipes. Figure (11) shows examples of the finite element meshes used for this purpose. It is important to note that coarse meshes are displayed in this figure, and the FEM simulations were actually performed using finer meshes.

The loading and boundary conditions for the FEM models of the lateral compression test are as follows:

Table 8
Results of the mesh independence study for the split-disk test.

Element size (mm)	Maximum von Mises stress in pipe (MPa)	Error (%)
2.0	97.0	31.4
1.0	141.4	16.8
0.5	170.0	5.4
0.25	179.7	1.1
0.10	181.7	0.4
0.05	182.4	–

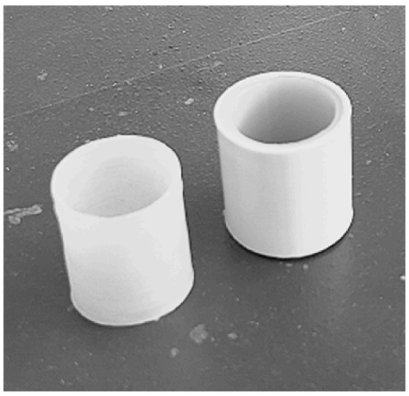

Fig. 9. Compression samples of PEX and PEX-Al-PEX pipes.

Fig. 10. Snapshots of the PEX-Al-PEX pipe compression at different time points.

- All degrees of freedom are fixed for the reference point of the rigid plate, denoted by number 1 in Figure (11), except for the y-displacement, which matches the vertical displacement of the test fixture.
- A y-symmetry boundary condition is applied to the pipe surface which is perpendicular to the y-axis and labeled as number 2 in Figure (11).
- An x-symmetry boundary condition is applied to the pipe surface which is perpendicular to the x-axis and marked as number 3 in Figure (11).
- A z-symmetry boundary condition is applied to the pipe surface which is perpendicular to the z-axis and shown as number 4 in Figure (11).

The force-displacement curves for the lateral compression of the single-layer PEX pipe obtained by the finite element model are compared with experimental data in figures (12) and (13) at different values of the testing machine crosshead speed and working temperature, respectively. According to these figure, the finite element predictions are in good agreement with results of the experimental tests in all simulated conditions.

The force-displacement curves for the lateral compression of the PEX-Al-PEX pipe obtained by the finite element model are compared with experimental data in figures (14) and (15) at different values of the testing machine crosshead speed and working temperature, respectively. According to these figures, the finite element model can predict the results of the experimental tests with good accuracy in all simulated conditions.

The deformed shapes of the PEX-Al-PEX pipe at a moment during lateral compression, at maximum compression with 16 mm displacement of compression fixtures, and after unloading are shown in Figure (16) for both experimental and finite element methods.

The distribution of the von-Mises stress in the multilayer pipe is shown in figure (17) at four different moments of the lateral compression test. It can be seen that the maximum stress occurs in the aluminum layer at every stage of the compression test.

3.2. Pipe split-disk tensile test

Another commonly used test for examining the mechanical properties of pipes is the split-disk tensile test defined by ASTM D2290 standard [58] used by several previous studies such as [59–61]. The split-disk test can be used as a simple alternative for the hydrostatic pressure test to determine the circumferential tensile strength and stiffness of the pipe. Compared with test methods like the hydrostatic burst test in which the whole products have to be tested, the split-disk test has advantages of simplicity, low cost and high efficiency [62].

In this testing method, the standard sample which has a loop-like shape is placed around the two halves of a split-disk. Each half of the disk is pulled by one of the jaws of the tensile testing machine until the sample breaks. This test is used to determine the tensile properties of the

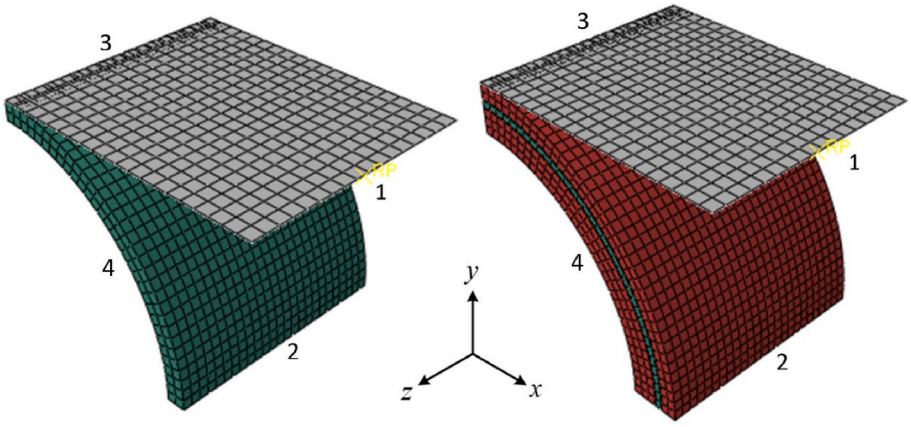

Fig. 11. Finite element meshes for lateral compression test of PEX and PEX-Al-PEX pipes.

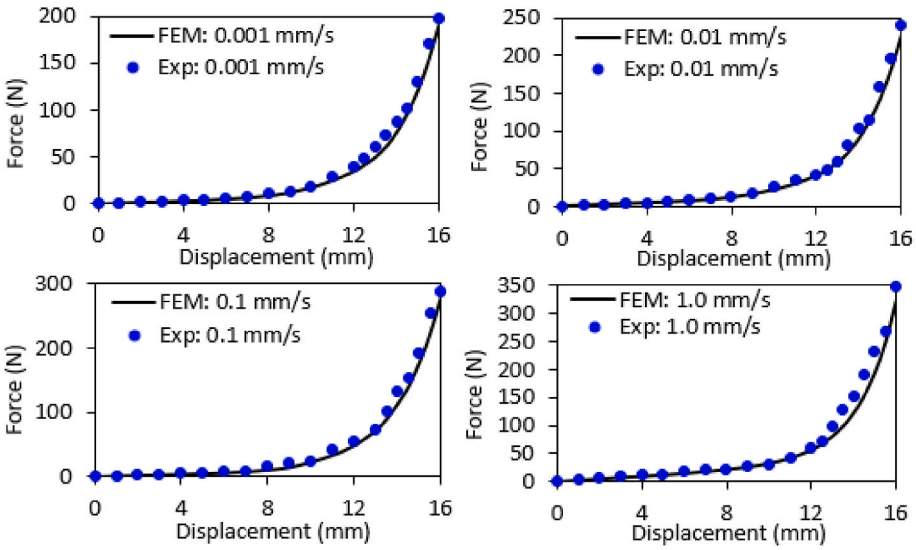

Fig. 12. Comparison of the finite element results and experimental data for lateral compression of PEX pipe at different speeds of the testing machine crosshead.

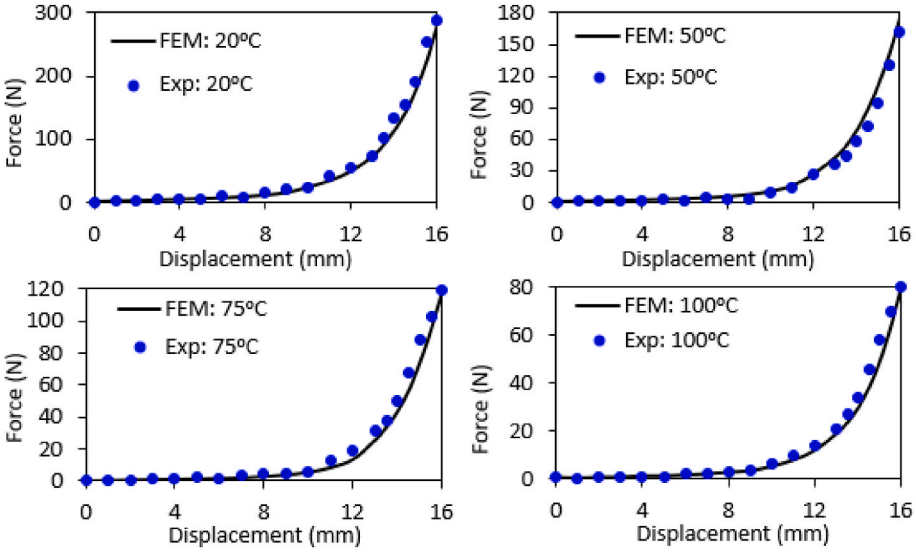

Fig. 13. Comparison of the finite element results and experimental data for lateral compression of PEX pipe at different working temperatures.

tube in the circumferential direction. The standard geometry of the sample and two samples made by CNC machining for PEX-Al-PEX and PEX pipes are presented in figure (18). Just like the lateral compression test, the thickness of the PEX pipe is 1 mm.

Two fixtures have been made along with two half disks to perform the split-disk test on a universal tensile test machine. The tests have been performed at T = 20°C for four different speeds (0.001, 0.01, 0.1, and 1.0 mm/s) of the compressive test fixture, and at different temperatures (20, 50, 75, 100°C) for fixture speed of 0.1 mm/s. Each test was repeated on five specimens to obtain a reliable average for a sample according to standard [58]. Two views of a mounted specimen for the split-disk test are provided in figure (19).

Figures (20) shows examples of the finite element models used for the split-disk test of PEX and PEX-Al-PEX pipes. In order to avoid excessive mesh distortion in the finite element simulation of the split-disk test, arbitrary Lagrangian -Eulerian (ALE) adaptive meshing strategy has been applied to the pipe layers.

The loading and boundary conditions for the FEM models of the split-disk test are as follows:

- All degrees of freedom are fixed for the reference point of the rigid tool, denoted by number 1 in Figure (20), except for the y-displacement, which matches the vertical displacement of the split-disk in the experimental test.
- A y-symmetry boundary condition is applied to the pipe surface which is perpendicular to the y-axis and labeled as number 2 in Figure (20).
- An x-symmetry boundary condition is applied to the pipe surface which is perpendicular to the x-axis and marked as number 3 in Figure (20).
- A z-symmetry boundary condition is applied to the pipe surface which is perpendicular to the z-axis and shown as number 4 in Figure (20).

The force-displacement curves for the single-layer PEX pipe are given in figures (21) and (22) at different values of the testing machine crosshead speed and working temperature, respectively. According to these figure, the finite element predictions are in good agreement with results of the experimental tests in all simulated conditions.

According to these figures, the force increases with displacement to a

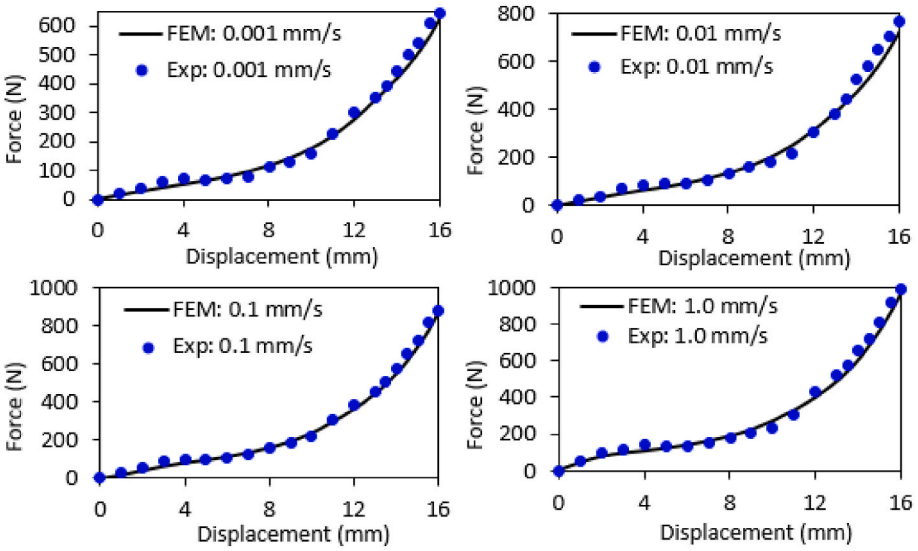

Fig. 14. Comparison of the finite element results and experimental data for lateral compression of PEX-Al-PEX pipe at different speeds of the testing machine crosshead.

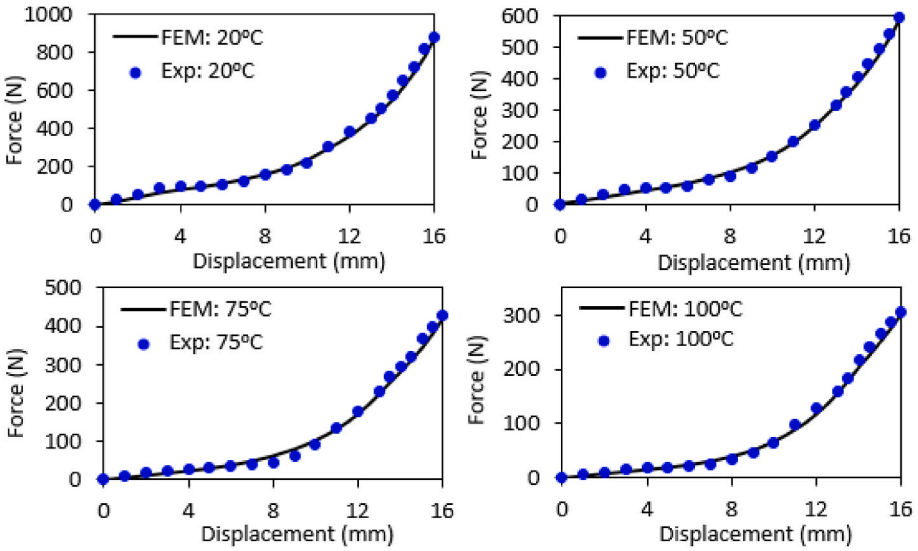

Fig. 15. Comparison of the finite element results and experimental data for lateral compression of PEX-Al-PEX pipe at different working temperatures.

Fig. 16. The deformed shape of the PEX-Al-PEX pipe at a point during the compression, at the maximum compression, and after unloading.

maximum value in all conditions, after which it suddenly drops to zero due to the rupture of the test specimen. Furthermore, the rupture force increases as the crosshead speed increases and the working temperature decreases. This can be attributed to the fact that the flow stress of the PEX rises with an increase in strain-rate and a decrease in temperature.

To discuss the damage evolution and rupture process in the PEX specimen, the distributions of the effective strain and von-Mises stress in the specimen obtained by the finite element method are analyzed here at some key moments of simulation. Only one of the simulations performed at the crosshead speed of 0.1 mm/s and working temperature of T =

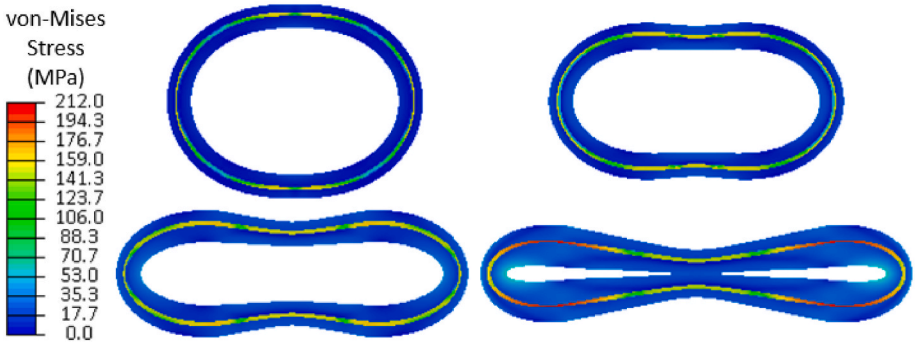

Fig. 17. The deformed shape of the PEX-Al-PEX pipe after removing the compressive load.

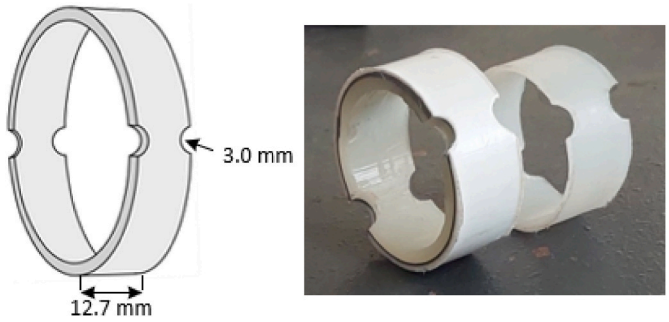

Fig. 18. Standard geometry of the sample, PEX-Al-PEX and PEX samples for split-disk test.

20°C is considered for the sake of brevity.

The contours of the von-Mises stress and effective strain in the PEX specimen just before the damage initiation are shown in figure (23). It is evident from this figure that the maximum values of both stress and strain occur at the edge of the hole located in the inner surface of the specimen. This location is the critical zone of the specimen which is subjected to the maximum stress and strain.

The contours of the von-Mises stress and effective strain in the specimen are displayed in figure (24) during the damage evolution at the brink of the rupture initiation. According to this figure, while the effective strain has increased in the critical zone, the von-Mises stress has decreased in this location. This is due to the fact that as deformation continues and damage grows in the specimen, the von-Mises stress decreases in the damaged elements according to equation (4).

The von-Mises stress decreases in the critical zone until the damage parameter reaches its critical value (equal to unity) and elements located at this zone are deleted since they are completely damaged and cannot sustain loads anymore. This condition which is the start of the specimen rupture process is shown in figure (25).

Different episodes of the specimen deformation before, during and after its rupture are displayed in figure (26). Based on this figure, during the rupture process more and more elements are completely damaged and deleted from the finite element model until two parts of the specimen are separated at its narrowest cross-section.

The force-displacement curves obtained by the experimental and finite element methods for the split-disk test of the PEX-Al-PEX pipe at different values of strain-rate and temperature are compared in figures (27) and (28), respectively. According to these figures, the finite element model can predict experimental data with reasonable accuracy.

As can be seen in these figures, the force increases with displacement in the elastic region and up to a certain point in the plastic region. Then, at a specific displacement, the force suddenly decreases to a lower level. After this drop, the force increases slightly again and ultimately drops to zero with another sudden decrease. To understand this behavior in the force-displacement diagram, it is necessary to examine the pipe's shape during the deformation process. For this purpose, the results of the finite element method will be used.

Figure (29) depicts the evolution of deformation in the multilayer pipe at various moments in time. The entire simulation duration was 20 s, and in this figure, the PEX material is denoted in purple, while the aluminum material is represented in green.

In accordance with figure (29), at $t = 11.22$ s the rupture process has not yet commenced in the pipe, and the force value in the force-displacement graph is still increasing. However, just a moment later, at $t = 11.24$ s, the rupture of the inner layer of the pipe initiates, and as figure (29) illustrates, it continues until $t = 13.88$ s when this layer completely fractures. In fact, the abrupt drop in force that occurs after the initial ascent in the force-displacement graph is a result of this rupture process in the inner layer of the pipe. It's worth noting that although the inner layer of the pipe withstands significantly less stress

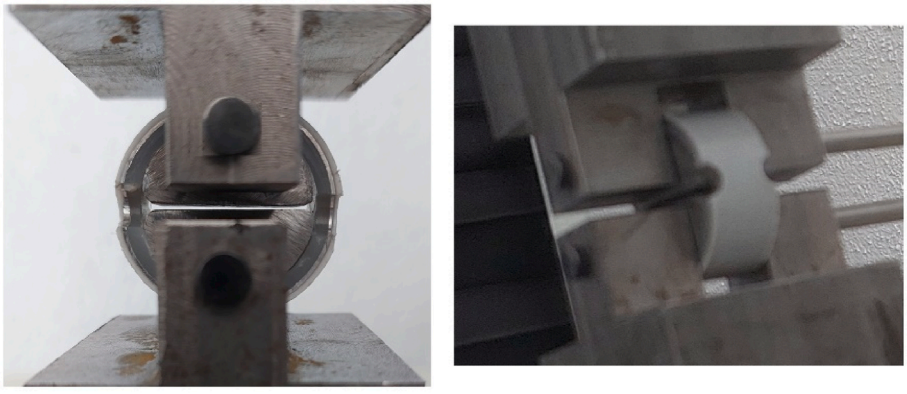

Fig. 19. Two views of a mounted specimen for the split-disk test.

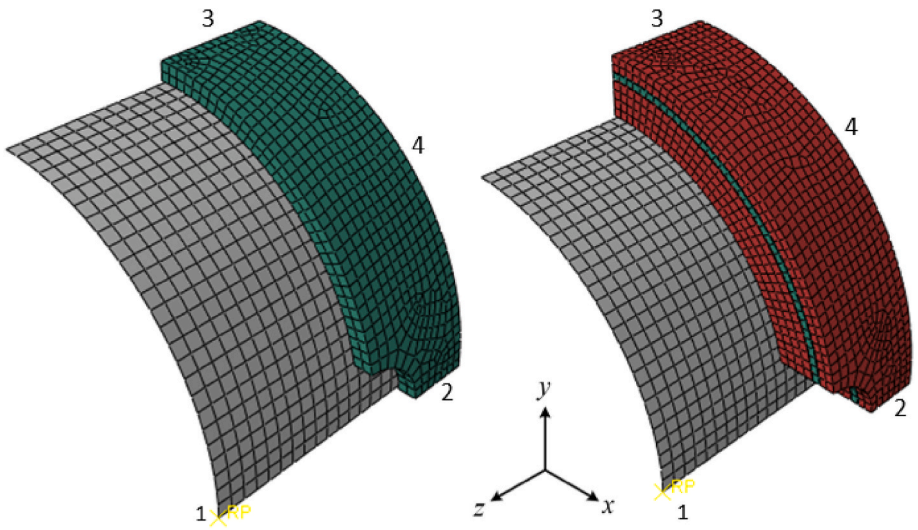

Fig. 20. Finite element models for the split-disk test of PEX and PEX-Al-PEX pipes.

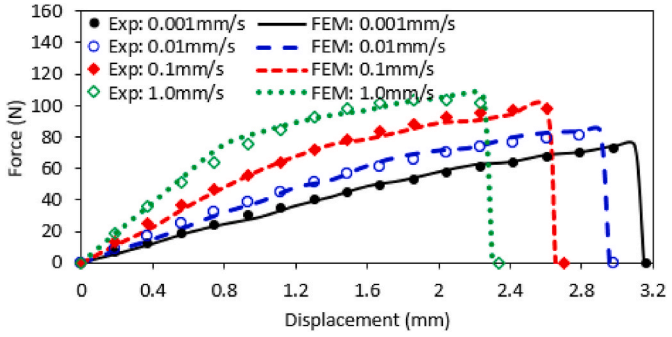

Fig. 21. Comparison of the force obtained by finite element and experimental methods in split-disk test of PEX pipe at different cross-head speeds.

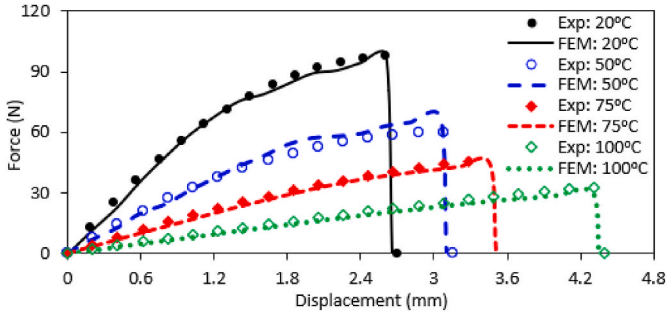

Fig. 22. Comparison of the force obtained by finite element and experimental methods in split-disk test of PEX pipe at different working temperatures.

compared to the aluminum layer, it bears a substantial portion of the force due to its larger cross-sectional area.

After the rupture of the inner layer, the force increases slightly due to the strain-hardening of the middle and outer layers of the pipe, up until the rupture process begins in these layers as well. To observe the continuation of the rupture process in the pipe, another view of pipe has been provided in figure (30).

In this figure, at $t = 15.94$ s, rupture has occurred solely in the inner layer, and it has not yet spread to the middle and outer layers. A moment later, at $t = 15.96$ s, the rupture process continues with the breaking of a portion of the outer layer. As depicted in the figure, at $t = 16.86$ s, sections of the middle layer of the pipe, along with the outer layer, have

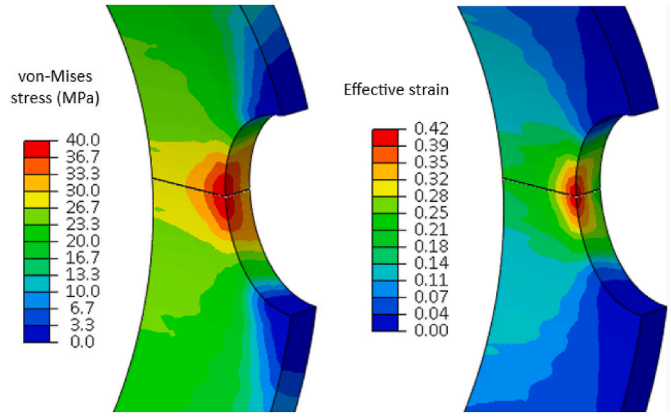

Fig. 23. The von-Mises stress and effective strain distribution in the PEX specimen just before damage initiation.

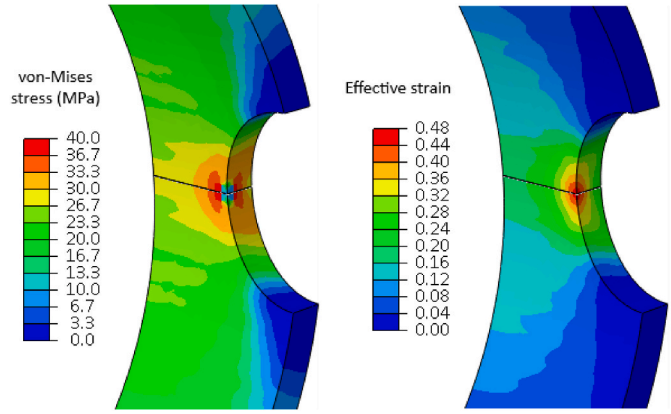

Fig. 24. The von-Mises stress and effective strain distribution in the PEX specimen during damage evolution.

experienced breaking. The process of rupture progresses over time, and at $t = 17.30$ s, more sections of the middle and outer layers have ruptured. At $t = 17.32$ s, the outer layer has completely broken, leaving only a small portion of the middle layer to bear the force. Finally, this remaining section also breaks a short while later at $t = 17.38$ s,

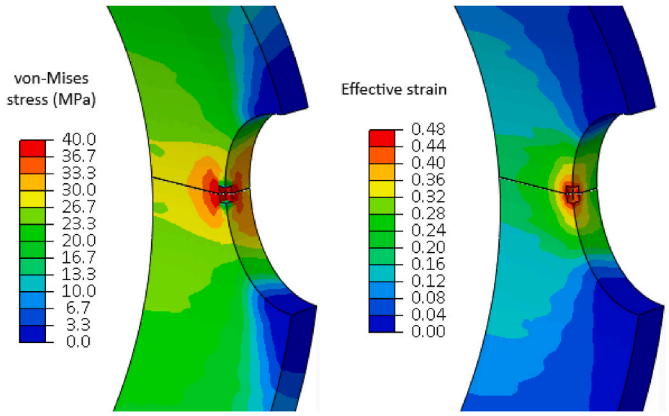

Fig. 25. The von-Mises stress and effective strain distribution in the PEX specimen at the start of the rupture process.

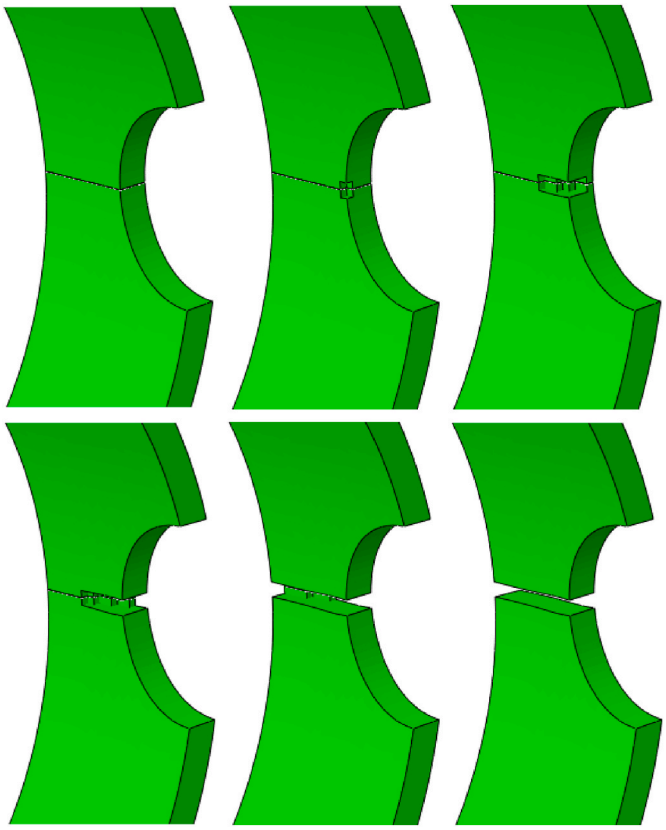

Fig. 26. Different episodes of the specimen deformation before, during and after its rupture.

resulting in the complete separation of the two pipe sections, and the force drops to zero.

An example of the von-Mises stress distribution in the pipe before the initiation of the rupture process is illustrated in figure (31). According to this figure, the highest stress is generated in the aluminum layer and then the inner layer, respectively, while the outer layer bears the lowest stress magnitude. However, due to the higher strength of aluminum compared to PEX, the aluminum layer is the last layer of the pipe to rupture.

3.3. Internal pressure loading

Given that the primary function of pipes is to transport various fluids,

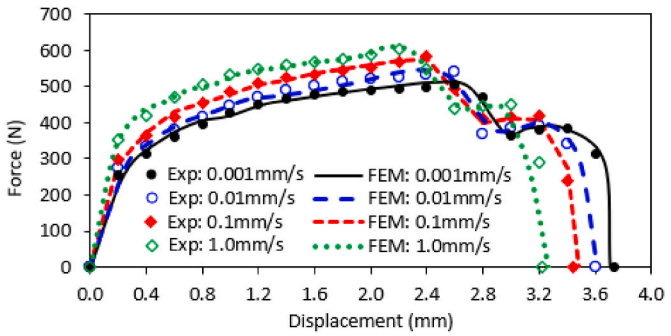

Fig. 27. Comparison of the force obtained by finite element and experimental methods in split-disk test of PEX-Al-PEX pipe at different crosshead speeds.

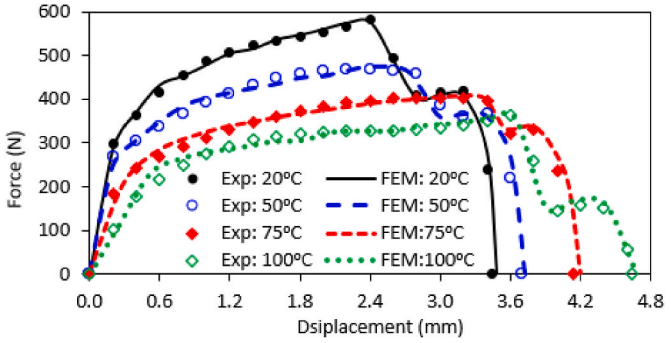

Fig. 28. Comparison of the force obtained by finite element and experimental methods in split-disk test of PEX-Al-PEX pipe at different working temperatures.

the internal pressure exerted by the fluid on the pipe is the most common load that the pipe experiences throughout its operational life. Therefore, in this section, the distribution of strain and stress in a PEX-Al-PEX pipe is investigated under internal pressure. The plumbing water pressure typically ranges between 276 and 552 kPa (40 and 80psi). Water pressure below 276 kPa is considered low, and water pressure above 552 kPa is considered too high [63,64]. In light of this consideration, the study has been conducted for these values of the internal pressure.

For the distributions of the radial and hoop stresses in the PEX-Al-PEX pipes, analytical solutions have been presented by Atarodi-Kashani et al. in Ref. [23] based on the classical elasticity theory. To further assess the validity of the finite element model, a comparison will be made between the stress predicted by the finite element method and the mentioned analytical approach. The distributions of the hoop and radial stresses in the radial direction of 2025 and 2532 pipes obtained by finite element and analytical methods are compared in figures (32) and (33) for internal pressures of 276 and 552 kPa.

As can be seen in these figures, the results of finite element and analytical methods are in relatively good agreement in all studied cases.

3.4. Significance and novelty of the results

Nowadays, PEX-AL-PEX pipes are increasingly used in industrial, agricultural, and domestic applications. However, to the authors' knowledge, apart from two articles that have examined the weld seam of the aluminum layer in these pipes [22,23], no studies have been published on the behavior of these pipes and their components. In this paper, suitable constitutive models that can predict the elastic, plastic, and mechanical damage behavior of various components of these pipes at different temperatures and strain-rates are introduced. Additionally, the method of modeling the layered structure of these pipes, where layers are bonded with adhesive, using the finite element method is explained. Using the developed model, the behavior of the pipe and its

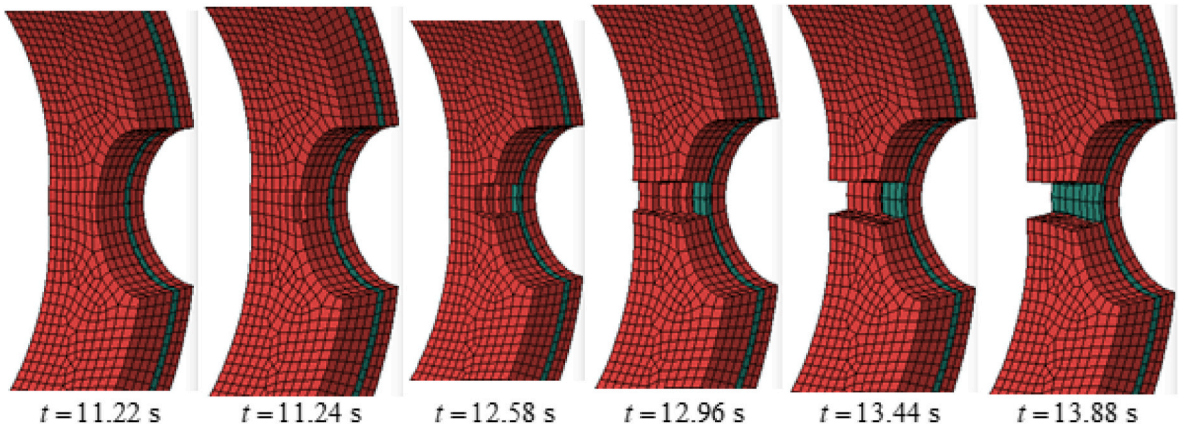

Fig. 29. The rupture process of the inner layer of the pipe.

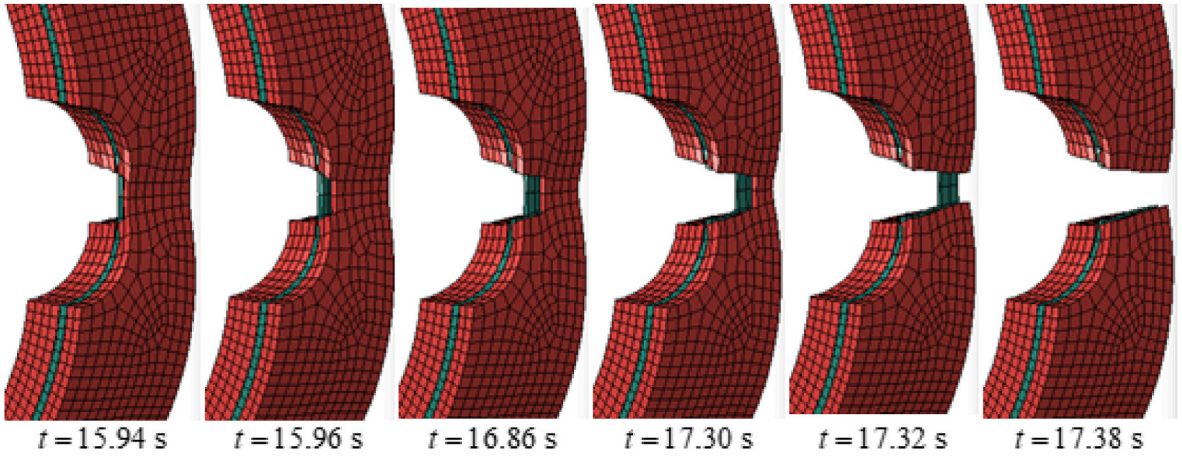

Fig. 30. The rupture process of the middle and outer layers of the pipe.

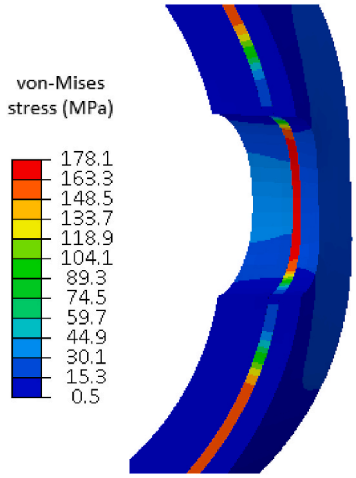

Fig. 31. An example of the von Mises stress distribution in the pipe before the initiation of the rupture process.

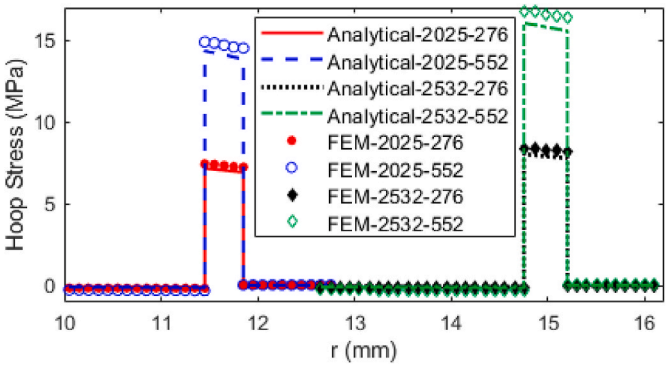

Fig. 32. Distribution of the hoop stress in the hoop direction of the pipes.

layers from the beginning of loading to the moment of final failure under various loading and operating conditions can be simulated. The failure process of the pipe and the sequence of rupture of its layers are also identified using damage mechanics in the finite element model, and the models of the pipe and its layers are extensively validated with experimental data. The aim of this comprehensive study is to reduce the gap in the literature regarding the examination of the properties and mechanical behavior of PEX-AL-PEX pipes, providing a modeling framework that will assist researchers and engineers in analyzing, designing, and optimizing these pipes.

4. Conclusion

In this paper, a finite element model was developed in the Abaqus/Explicit software to study the mechanical behavior of PEX-AL-PEX pipes under various strain-rates and temperatures. The properties of different layers of the pipe were obtained either from appropriate experimental

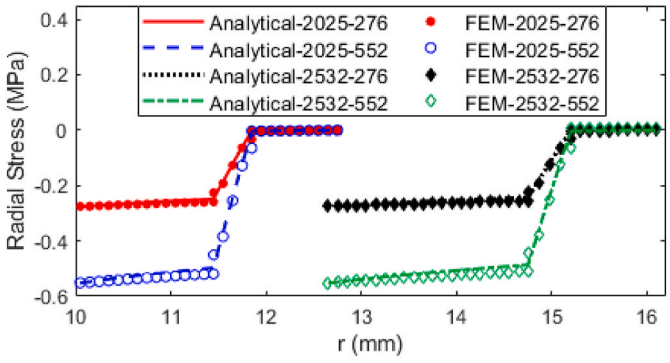

Fig. 33. Distribution of the hoop stress in the radial direction of the pipes.

tests or from their respective manufacturers. Experimental results showed that the elastic modulus, yield strength, and tangential modulus follow power-law relationships with strain-rate and exponential relationships with temperature for PEX material. Since such a material behavior is not available as a default in the Abaqus library, a VUMAT subroutine was developed to define the material properties. For modeling aluminum, an elastic-plastic behavior with linear strain-hardening was used. The plastic behavior of aluminum, as well as its damage behavior, was implemented using the Johnson-Cook material model, which can describe the strain-rate and temperature dependence. To evaluate the accuracy of the developed model, the lateral compression and the split-disk tension tests were performed following the relevant standards. The tests were performed at different temperatures and strain-rates, and the force-displacement curves were obtained. Simulation of these tests using the finite element method and comparison of the results with experimental data under different working conditions demonstrated that the developed model had reasonable accuracy.

CRediT authorship contribution statement

Ameer Alaa Oleiwi: Writing – original draft, Visualization, Validation, Software, Methodology, Investigation, Formal analysis, Data curation. **Hamed Afrasiab:** Writing – review & editing, Writing – original draft, Visualization, Validation, Supervision, Software, Resources, Project administration, Methodology, Investigation, Formal analysis, Data curation, Conceptualization. **Abbas Zolfaghari:** Supervision, Investigation, Formal analysis.

Declaration of competing interest

The authors declare that they have no known competing financial interests or personal relationships that could have appeared to influence the work reported in this paper.

Data availability

Data will be made available on request.

References

[1] D. Zeng, X. Wang, K. Ming, C. Yu, Y. Zhang, Z. Yu, J. Yan, F. Li, Analysis and optimization design of internal pressure resistance of flexible composite pipe, Int. J. Press. Vessels Pip. 210 (2024) 105271, https://doi.org/10.1016/j.ijpvp.2024.105271.

[2] T. Gu, Z. Lian, Y. Dou, Z. Wu, G. Li, Simulation and experimental study on liner collapse of lined composite pipe, Int. J. Press. Vessels Pip. 207 (2024) 105106, https://doi.org/10.1016/j.ijpvp.2023.105106.

[3] E. Naeiji, H. Afrasiab, Analyzing mechanical properties and loading performance of polypropylene sandwich pipes, J. Sandw. Struct. Mater. 26 (2024) 1037–1059, https://doi.org/10.1177/10996362241251808.

[4] G. Schumacher da Silva, B.N. Rojo Tanzi, G. Giordani, E.B. Groth, M. Roland Sobczyk, I. Iturrioz, L. de Abreu Corrêa, Analysis of the dispersive behavior of polymer-coated steel two-phase pipes, Thin-Walled Struct. 184 (2023) 110467, https://doi.org/10.1016/j.tws.2022.110467.

[5] S. Li, S. Zou, L. Dai, Y. Zhou, X. Qiu, C. Li, P. Li, T. Jo Ko, Damage mechanism of carbon-fiber-reinforced-plastic pipe based on reverse and forward curvature drilling, Compos. Struct. 292 (2022) 115701, https://doi.org/10.1016/j.compstruct.2022.115701.

[6] L. Li, X. Niu, B. Han, L. Song, X. Li, Microstructure and properties of laser cladding coating at the end of L415/316L bimetal composite pipe, Int. J. Press. Vessels Pip. 195 (2022) 104568, https://doi.org/10.1016/j.ijpvp.2021.104568.

[7] X. Dong, E.R. Malta, H. Shiri, Deformation of trenched multilayer pipelines during large lateral displacement due to subsea geohazards, Ocean Eng 278 (2023) 114352, https://doi.org/10.1016/j.oceaneng.2023.114352.

[8] Y. He, M.A. Vaz, M. Caire, M. Duan, J. Su, Transient thermomechanical axisymmetric analysis of multilayer thermoplastic composite pipes, Appl. Math. Model. 124 (2023) 257–278, https://doi.org/10.1016/j.apm.2023.08.001.

[9] R. Rajasekar, K.S.K. Sasi Kumar, P. Sathish Kumar, Multi layer pipes, in: J.K. Kim, S. Thomas, P. Saha (Eds.), Multicomponent Polym. Mater., Springer, Netherlands, Dordrecht, 2016, pp. 279–299, https://doi.org/10.1007/978-94-017-7324-9_10.

[10] M.J.S. Patil, Analysis of multilayered composite pipe under internal pressure using finite element methodology, Int. J. Res. Appl. Sci. Eng. Technol. 7 (2019) 3772–3778, https://doi.org/10.22214/ijraset.2019.4633.

[11] H. Afrasiab, M.R. Movahhedy, A. Assempour, Finite element and analytical fluid-structure interaction analysis of the pneumatically actuated diaphragm microvalves, Acta Mech. 222 (2011) 175, https://doi.org/10.1007/s00707-011-0508-9.

[12] H. Afrasiab, M.R. Movahhedy, Treatment of the small time instability in the finite element analysis of fluid structure interaction problems, Int. J. Numer. Methods Fluids 71 (2013) 756–771.

[13] P. Hutař, L. Náhlík, L. Šestáková, M. Ševčík, Z. Knésl, E. Nezbedová, A fracture mechanics assessment of surface cracks existing in protective layers of multi-layer composite pipes, Compos. Struct. 92 (2010) 1120–1125, https://doi.org/10.1016/j.compstruct.2009.10.004.

[14] U. Niedermayer, O. Boine-Frankenheim, Analytical and numerical calculations of resistive wall impedances for thin beam pipe structures at low frequencies, Nucl. Instrum. Methods Phys. Res. Sect. Accel. Spectrometers Detect. Assoc. Equip. 687 (2012) 51–61, https://doi.org/10.1016/j.nima.2012.05.096.

[15] L.L. Aguiar, C.A. Almeida, G.H. Paulino, A three-dimensional multilayered pipe beam element: nonlinear analysis, Comput. Struct. 138 (2014) 142–161, https://doi.org/10.1016/j.compstruc.2013.09.005.

[16] H. Yazdani Sarvestani, M. Hojjati, Three-dimensional stress analysis of orthotropic curved tubes-part 2: laminate solution, Eur. J. Mech. - ASolids 60 (2016) 339–358, https://doi.org/10.1016/j.euromechsol.2016.06.004.

[17] Y. Bai, S. Yuan, P. Cheng, P. Han, W. Ruan, G. Tang, Confined collapse of unbonded multi-layer pipe subjected to external pressure, Compos. Struct. 158 (2016) 1–10, https://doi.org/10.1016/j.compstruct.2016.09.007.

[18] S. Hartmann, J. Mohan, L. Müller-Lohse, B. Hagemann, L. Ganzer, An analytical solution of multi-layered thick-walled tubes in thermo-elasticity with application to gas-wells, Int. J. Press. Vessels Pip. 161 (2018) 10–16, https://doi.org/10.1016/j.ijpvp.2018.01.001.

[19] P. Wu, M. Wang, H. Fang, Exact solution for infinite multilayer pipe bonded by viscoelastic adhesive under non-uniform load, Compos. Struct. 259 (2021) 113240, https://doi.org/10.1016/j.compstruct.2020.113240.

[20] Z. Zhang, D. Zhou, Y.M. Lim, H. Fang, R. Huo, Analytical solutions for multilayered pipes with temperature-dependent properties under non-uniform pressure and thermal load, Appl. Math. Model. 106 (2022) 369–389, https://doi.org/10.1016/j.apm.2022.01.024.

[21] L. Trávníček, J. Poduška, M. Messiha, F. Arbeiter, G. Pinter, L. Náhlík, P. Hutař, Effect of recycled material on failure by slow crack growth in multi-layer polyethylene pipes, Eng. Fract. Mech. 289 (2023) 109423, https://doi.org/10.1016/j.engfracmech.2023.109423.

[22] M. Riahi, N. Ebrahimi, Test apparatus for on-line butt-welding evaluation of aluminum layer in PEX-AL-PEX multilayer pipes, Exp. Tech. 40 (2016) 185–193, https://doi.org/10.1007/s40799-016-0023-y.

[23] A. Atarodi-Kashani, S. Delfani, M. Khademi, M. Shafaie, Investigation of long-term rupture pressure in PEX-AL-PEX composite pipes, Int. J. Press. Vessels Pip. 200 (2022) 104790, https://doi.org/10.1016/j.ijpvp.2022.104790.

[24] F17 Committee, Specification for Crosslinked Polyethylene/Aluminum/Crosslinked Polyethylene (PEX-AL-PEX) Pressure Pipe, ASTM International, n.d. https://doi.org/10.1520/F1281-17R21E01.

[25] E28 Committee, Test Methods for Tension Testing of Metallic Materials, ASTM International, n.d. https://doi.org/10.1520/E0008_E0008M-21.

[26] J.Q. Tan, M. Zhan, S. Liu, T. Huang, J. Guo, H. Yang, A modified Johnson–Cook model for tensile flow behaviors of 7050-T7451 aluminum alloy at high strain rates, Mater. Sci. Eng. A 631 (2015) 214–219, https://doi.org/10.1016/j.msea.2015.02.010.

[27] D.-N. Zhang, Q.-Q. Shangguan, C.-J. Xie, F. Liu, A modified Johnson–Cook model of dynamic tensile behaviors for 7075-T6 aluminum alloy, J. Alloys Compd. 619 (2015) 186–194, https://doi.org/10.1016/j.jallcom.2014.09.002.

[28] S. Akram, S.H.I. Jaffery, M. Khan, M. Fahad, A. Mubashar, L. Ali, Numerical and experimental investigation of Johnson–Cook material models for aluminum (Al 6061-T6) alloy using orthogonal machining approach, Adv. Mech. Eng. 10 (2018) 1687814018797794, https://doi.org/10.1177/1687814018797794.

[29] S. Gupta, S. Abotula, A. Shukla, Determination of johnson–cook parameters for cast aluminum alloys, J. Eng. Mater. Technol. 136 (2014), https://doi.org/10.1115/1.4027793.

[30] H. Afrasiab, Numerical and analytical approaches for improving the die design in the radial forging process of tubes without mandrel, Sci. Iran. 23 (2016) 167–173.
[31] M. Xu, G. Huang, S. Feng, X. Qin, G.J. McShane, W.J. Stronge, Perforation resistance of aluminum/polyethylene sandwich structure, Mater. Des. 100 (2016) 92–101, https://doi.org/10.1016/j.matdes.2016.03.090.
[32] R. Jain, S.K. Pal, S.B. Singh, 5 - numerical modeling methodologies for friction stir welding process, in: J. Paulo Davim (Ed.), Comput. Methods Prod. Eng., Woodhead Publishing, 2017, pp. 125–169, https://doi.org/10.1016/B978-0-85709-481-0.00005-7.
[33] S. Pandre, A. Morchhale, N. Kotkunde, S.K. Singh, N. Khanna, A. Saxena, Chapter Three - experimental and numerical investigation of deformation behavior of dual phase steel at elevated temperatures using various constitutive models and ANN, in: K. Kumar, G. Kakandikar, J.P. Davim (Eds.), Comput. Intell. Manuf., Woodhead Publishing, 2022, pp. 47–70, https://doi.org/10.1016/B978-0-323-91854-1.00008-X.
[34] H. Afrasiab, M.G. Hamzekolaei, A. Hassani, New insight into the radial forging process by an asymptotic-based axisymmetric analysis, Appl. Math. Model. 102 (2022) 811–827, https://doi.org/10.1016/j.apm.2021.10.030.
[35] D.E. Schick, Characterization of Aluminum 3003 Ultrasonic Additive Manufacturing, The Ohio State University, 2009. https://etd.ohiolink.edu/apexprod/rws_olink/r/1501/10?clear=10&p10_accession_num=osu1259773538. (Accessed 18 July 2023).
[36] A. Siddiq, E. Ghassemieh, Theoretical and FE analysis of ultrasonic welding of aluminum alloy 3003, J. Manuf. Sci. Eng. 131 (2009), https://doi.org/10.1115/1.3160583.
[37] E. Alaei, H. Afrasiab, M. Dardel, Analytical and numerical fluid–structure interaction study of a microscale piezoelectric wind energy harvester, Wind Energy 23 (2020) 1444–1460, https://doi.org/10.1002/we.2502.
[38] H.H. Xu, H.C. Luo, X.G. Zhang, W. Jiang, X.C. Teng, W.Q. Chen, J. Yang, Y.M. Xie, X. Ren, Mechanical properties of aluminum foam filled re-entrant honeycomb with uniform and gradient designs, Int. J. Mech. Sci. 244 (2023) 108075, https://doi.org/10.1016/j.ijmecsci.2022.108075.
[39] J. Xiang, Y. Wang, Y. Wu, Q. Peng, L. Shui, W. Ouyang, T. Ding, Z. Liu, Superplastic nanomolding of highly ordered metallic sub-micrometer pillars arrays for surface enhanced Raman scattering, Adv. Mater. Technol. 7 (2022) 2100891, https://doi.org/10.1002/admt.202100891.
[40] G. Gao, E. Tang, M. Feng, Y. Han, Y. Li, M. Liu, Y. Xu, L. Wang, X. Lin, R. Wang, Y. Cheng, L. Zhao, Z. Liang, J. Wang, G. Zhao, Q. Gao, T. Zheng, Research on dynamic response characteristics of CFRP/Al HC SPs subjected to high-velocity impact, Def. Technol. 14 (2018) 503–512, https://doi.org/10.1016/j.dt.2018.06.017.
[41] H. Afrasiab, K.H. Davoodi, M.M. Barzegari, M. Gholami, A. Hassani, A novel constitutive stress-strain law for compressive deformation of the gas diffusion layer, Int. J. Hydrog. Energy (2022), https://doi.org/10.1016/j.ijhydene.2022.07.127. S0360319922031780.
[42] D.B. Barry, O. Delatycki, The strain rate dependency of fracture in polyethylene: fracture initiation, J. Appl. Polym. Sci. 38 (1989) 339–350, https://doi.org/10.1002/app.1989.070380215.
[43] L.E. Govaert, T. Peijs, Tensile strength and work of fracture of oriented polyethylene fibre, Polymer 36 (1995) 4425–4431, https://doi.org/10.1016/0032-3861(95)96848-3.
[44] E.N. Brown, R.B. Willms, G.T. Gray, P.J. Rae, C.M. Cady, K.S. Vecchio, J. Flowers, M.Y. Martinez, Influence of molecular conformation on the constitutive response of polyethylene: a comparison of HDPE, uhmwpe, and PEX, Exp. Mech. 47 (2007) 381–393, https://doi.org/10.1007/s11340-007-9045-9.
[45] M. Amjadi, A. Fatemi, Tensile behavior of high-density polyethylene including the effects of processing technique, thickness, temperature, and strain rate, Polymers 12 (2020) 1857, https://doi.org/10.3390/polym12091857.
[46] X. Liu, W. Yu, Evaluation of the tensile properties and thermal stability of ultrahigh-molecular-weight polyethylene fibers, J. Appl. Polym. Sci. 97 (2005) 310–315, https://doi.org/10.1002/app.21720.
[47] J. Johnsen, F. Grytten, O.S. Hopperstad, A.H. Clausen, Influence of strain rate and temperature on the mechanical behaviour of rubber-modified polypropylene and cross-linked polyethylene, Mech. Mater. 114 (2017) 40–56, https://doi.org/10.1016/j.mechmat.2017.07.003.
[48] D20 Committee, Test Method for Tensile Properties of Plastics, ASTM International, n.d. https://doi.org/10.1520/D0638-14.
[49] ABAQUS User's Manual, 2012, Version 6.12.
[50] M.W. Joosten, M. Dingle, A. Mouritz, A.A. Khatibi, S. Agius, C.H. Wang, A hybrid embedded cohesive element method for predicting matrix cracking in composites, Compos. Struct. 136 (2016) 554–565, https://doi.org/10.1016/j.compstruct.2015.10.030.
[51] B. Attaf, Advances in Composite Materials: Ecodesign and Analysis, BoD – Books on Demand, 2011.
[52] Z. Zou, H. Lee, A cohesive zone model taking account of the effect of through-thickness compression, Compos. Part Appl. Sci. Manuf. 98 (2017) 90–98, https://doi.org/10.1016/j.compositesa.2017.03.015.
[53] A.M. Elmarakbi, N. Hu, H. Fukunaga, Finite element simulation of delamination growth in composite materials using LS-DYNA, Compos. Sci. Technol. 69 (2009) 2383–2391, https://doi.org/10.1016/j.compscitech.2009.01.036.
[54] Y.J.M. Brechet, Creep behavior of materials: a comparison, in: K.H.J. Buschow, R. W. Cahn, M.C. Flemings, B. Ilschner, E.J. Kramer, S. Mahajan, P. Veyssière (Eds.), Encycl. Mater. Sci. Technol., Elsevier, Oxford, 2001, pp. 1759–1765, https://doi.org/10.1016/B0-08-043152-6/00317-X.
[55] S. Lipa, M. Kotełko, Lateral impact of tubular structure – theoretical and experimental analysis. Part 1 – investigation of single tube, J. Theor. Appl. Mech. 51 (2013) 873–882.
[56] S. Eyvazinejad Firouzsalari, D. Dizhur, K. Jayaraman, N. Chouw, J.M. Ingham, Flax fabric-reinforced epoxy pipes subjected to lateral compression, Compos. Struct. 244 (2020) 112307, https://doi.org/10.1016/j.compstruct.2020.112307.
[57] T. Marsden, M. Stirling, C. Lang, High temperature test method for polymer pipes, Polym. Test. 68 (2018) 309–314, https://doi.org/10.1016/j.polymertesting.2018.04.008.
[58] F17 Committee, Test Method for Apparent Hoop Tensile Strength of Plastic or Reinforced Plastic Pipe, ASTM International, n.d. https://doi.org/10.1520/D2290-19A.
[59] H. Jemii, A. Bahri, A. Boubakri, D. Hammiche, K. Elleuch, N. Guermazi, On the mechanical behaviour of industrial PVC pipes under pressure loading: experimental and numerical studies, J. Polym. Res. 27 (2020) 240, https://doi.org/10.1007/s10965-020-02222-1.
[60] E.P. B, N.G. Tsouvalis, Finite element analysis of filament wound composite materials split disk tests, in: Adv. Anal. Des. Mar. Struct., CRC Press, 2023.
[61] Y. Kepir, A. Gunoz, M. Kara, Nonpenetrating repeated impact effect to the damage behavior of prestressed glass/epoxy composite pipes, Polym. Compos. 43 (2022) 5047–5058, https://doi.org/10.1002/pc.26777.
[62] Y. Zhao, P. Druzhinin, J. Ivens, D. Vandepitte, S.V. Lomov, Split-disk test with 3D Digital Image Correlation strain measurement for filament wound composites, Compos. Struct. 263 (2021) 113686, https://doi.org/10.1016/j.compstruct.2021.113686.
[63] S.D. Rhoades, Water systems standards survey, J. AWWA (Am. Water Works Assoc.) 78 (1986) 30–34, https://doi.org/10.1002/j.1551-8833.1986.tb05843.x.
[64] N.Y. Aydin, L. Mays, T. Schmitt, Sustainability assessment of urban water distribution systems, Water Resour. Manag. 28 (2014) 4373–4384, https://doi.org/10.1007/s11269-014-0757-1.